Vimentin binds to SARS-CoV-2 spike protein and antibodies targeting extracellular vimentin block *in vitro* uptake of SARS-CoV-2 virus-like particles

Łukasz Suprewicz [1] *, Maxx Swoger [2]*, Sarthak Gupta[2], Ewelina Piktel[1], Fitzroy J. Byfield [3], Daniel V. Iwamoto [3], Danielle A. Germann [2], Joanna Reszeć[4], Natalia Marcińczyk [5], Paul Janmey [3], J.M. Schwarz [1,6], Robert Bucki [1,3] **, Alison Patteson [2] **

1- Department of Medical Microbiology and Nanobiomedical Engineering, Medical University of Białystok, Poland
2- Physics Department and BioInspired Institute, Syracuse University
3- Institute for Medicine and Engineering and Department of Physiology, University of Pennsylvania
4- Department of Medical Pathomorphology, Medical University of Białystok, PL-15269 Białystok, Poland
5- Department of Biopharmacy, Medical University of Białystok, Białystok, Poland
6- Indian Creek Farm, Ithaca, NY

* Co-First authors
** Co-Corresponding authors

Abstract: Infection of human cells by pathogens, including SARS-CoV-2, typically proceeds by cell surface binding to a crucial receptor. In the case of SARS-CoV-2, angiotensin-converting enzyme 2 (ACE2) has been identified as a necessary receptor, but not all ACE2-expressing cells are equally infected, suggesting that other extracellular factors are involved in host cell invasion by SARS-CoV-2. Vimentin is an intermediate filament protein that is increasingly recognized as being present on the extracellular surface of a subset of cell types, where it can bind to and facilitate pathogens' cellular uptake. Here, we present evidence that extracellular vimentin might act as a critical component of the SARS-CoV-2 spike protein-ACE2 complex in mediating SARS-CoV-2 cell entry. We demonstrate direct binding between vimentin and SARS-CoV-2 virus-like particles coated with the SARS-CoV-2 spike protein and show that antibodies against vimentin block *in vitro* SARS-CoV-2 pseudovirus infection of ACE2-expressing cell lines. Our results suggest new therapeutic strategies for preventing and slowing SARS-CoV-2 infection, focusing on targeting cell host surface vimentin.

I. Introduction

Infection of human cells by pathogens, including SARS-CoV-2, proceeds by a series of cell surface protein binding and membrane fusion events that are usually centered on a crucial receptor. The SARS-CoV-2 virus is genetically similar to SARS-CoV (SARS) and uses the SARS receptor, angiotensin-converting enzyme 2 (ACE2), for cell entry (*1, 2*). The ACE2 receptor is expressed in the lung, kidney, gastrointestinal tract, and vascular endothelium, which all serve as sites for SARS-CoV-2 infection. While ACE2 seems to be required for SARS and SARS-CoV-2 infection, it does not appear solely sufficient. The expression of ACE2 in the human respiratory system is low compared to other organs (*3-5*) and while the affinity of the SARS-CoV2 spike protein with ACE is especially strong, the binding-on rate is slow (*1, 6*). At the super-physiological concentrations above nM used *in vitro*, the half time of maximal binding for SARS-CoV-2 is around 30 s, and the concentration in vivo is substantially lower. These findings have given rise to an emerging hypothesis of critical co-receptor that facilitate binding of the SARS virus and its delivery to ACE2 (*7*), and several possible SARS-CoV-2 co-receptors candidates have been found, including neuropilins (*8*), heparan sulfate (*9*), and sialic acids (*10*). The ongoing COVID-19 pandemic and the threat of future coronavirus outbreaks underscore the urgent need to identify the precise entry mechanism used by the SARS-CoV-2 virus to develop protective strategies against them.

Here, we report that cell surface vimentin acts as a critical co-receptor for SARS-CoV-2 host cell invasion and that antibodies against vimentin can block up to 80% of the cellular uptake of SARS-CoV-2 pseudovirus. While cell surface vimentin is an unconventional target for viruses, there are now numerous studies implicating its role in the binding and uptake of multiple different viruses (*11-18*), including the SARS virus (*19*), suggesting it might also be involved in cell host invasion by SARS-CoV-2. Interestingly, the expression of SARS-CoV-2 entry factors, ACE2 and TMPRSS2, is particularly high in nasal epithelial goblet secretory cells and ciliated cells (*20, 21*), on which immunohistological studies have shown the presence of vimentin (*22*). We show here that extracellular vimentin is also present in healthy adult lung tissue and detail the numerous routes by which it might arise in the lung, the respiratory track, and other tissues. We demonstrate that vimentin binds to SARS-CoV-2 virus-like particles (VLPs) that are equipped with SARS-CoV-2 spike 2 protein via dynamic light scattering and atomic force microscopy and propose a novel mechanism in which non-vimentin expressing cells can acquire vimentin released into the extracellular environment by neutrophil netosis. Our work critically highlights extracellular vimentin as a potential target against SARS-CoV-2 that could block the spread of COVID-19 and potentially other infectious diseases caused by viruses and bacteria that exploit cell surface vimentin for host invasion.

II. Results

a. Presence of extracellular vimentin in human lung, airway fluids, and fat tissue.

Vimentin is an unexpected target for SARS-CoV-2 viral entry into host cells lining the nasal and lung epithelial airways (Figure 1). Intermediate filaments (IFs) are categorized into five types based on similarities in sequence, which also exhibit similarities in tissue origin (*23, 24*). Keratin is the main IF protein expressed in epithelial cells, whereas vimentin is expressed in mesenchymal cells such as fibroblasts, endothelial cells and leukocytes. While vimentin is not nascently expressed in epithelial cells, its expression can occur in transformed cells associated with cancer, fibrosis, or immortalized cell lines.

There are however many routes by which vimentin might occupy the extracellular space of lung and other tissues. Lung epithelial cells are capable of expressing vimentin. This occurs, for instance, if the cell becomes fibrotic, cancerous, or undergoes the epithelial to mesenchymal transition. However, the source of extracellular vimentin need not be the lung epithelial cell itself, as other cell types have active mechanisms for releasing vimentin into the extracellular space (Fig. 1). This especially includes neutrophils (*25, 26*) macrophages (*27*), and endothelial cells (*28, 29*). While early studies have attributed extracellular vimentin to cytoskeletal debris and disruptions in the plasma membrane, it is now clear that it appears in the absence of cell damage (*30*). Furthermore, cell surface vimentin has biological functions in signaling between cell types and in infection by bacteria and viruses (*31, 32*).

The presence of vimentin on the surface of alveolar pneumonocytes and in the extracellular space of the lungs was assessed with an anti-vimentin antibody by immunostaining healthy lung parenchyma without pathology and sputum samples collected from the respiratory tract of cystic fibrosis patients (Fig. 1a). The presence of vimentin on the apical surface of type I and type II pneumocytes, cells without endogenous vimentin expression, indicate its extracellular origin. Immunostaining of airway sputum from cystic fibrosis patients showed the presence of vimentin in DNA-rich aggregate structures. Since obesity was identified as an important risk factor for complications in patients that suffered from SARS-CoV-2 infection (*33*), we also assessed the presence of vimentin in human adipose tissue (Fig. 1a). Indeed, vimentin expression was present in the stromal tissue, not in the adipocytes. The identification of extracellular vimentin in lung, sputum, and adipose tissue indicates a surprising pattern of extracellular vimentin presence in interstitial tissue and its possible role in SARS-CoV-2 uptake in lung and other ACE2 expressing tissues.

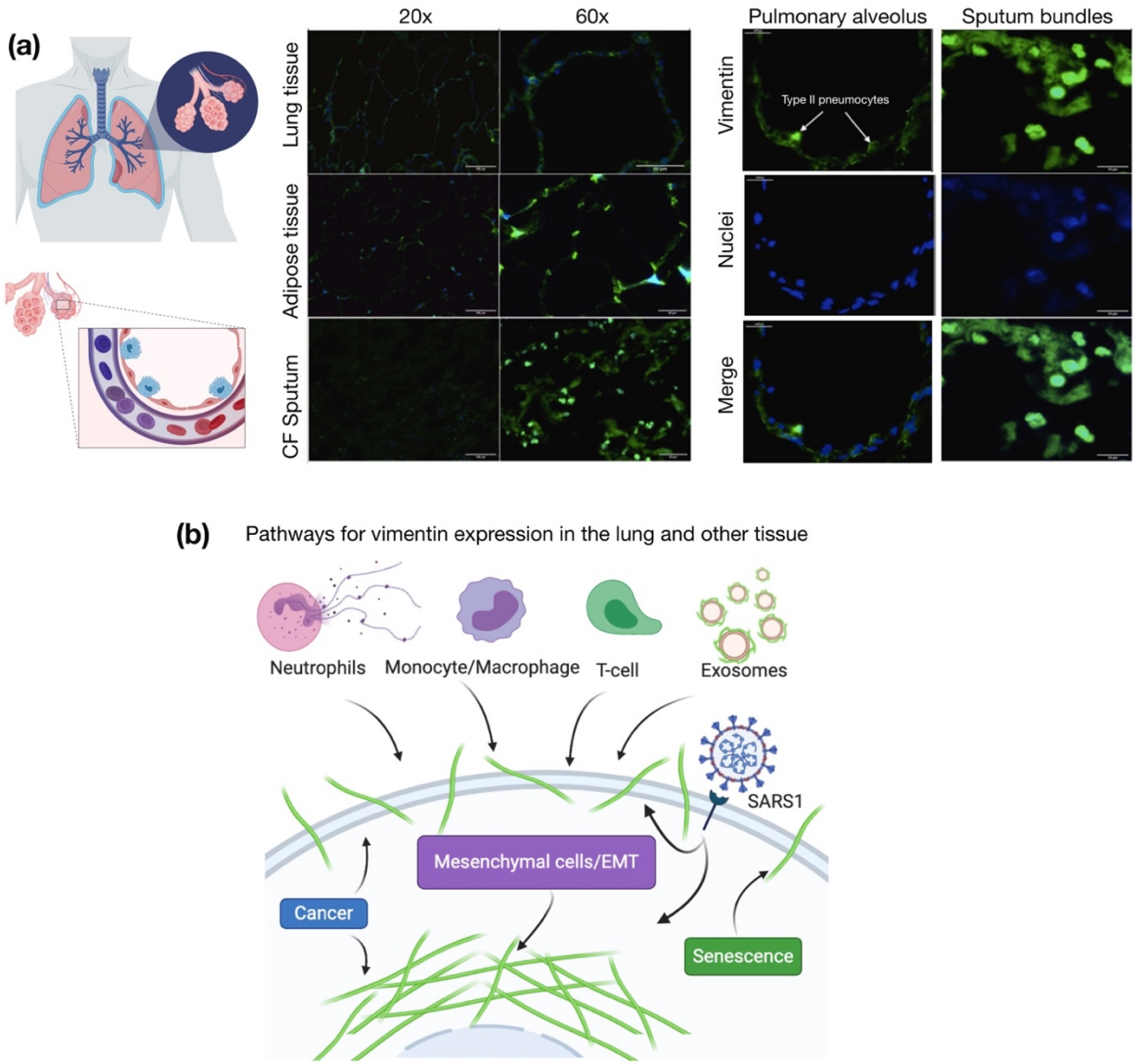

Figure 1. Presence of extracellular vimentin in human lung, airway fluids, and fat tissue. (a) Positive staining for extracellular vimentin (green) in human lung, fat tissue, and sputum obtained from cystic fibrosis (CF) patients. Vimentin appears on the apical side of type I and type II pneumocytes. DNA stained with DAPI. **(b)** There are numerous internal and exogenous pathways by which vimentin may be found in lung epithelia and other tissues, in either intracellular or cell surface forms (shown as green filaments). Vimentin is expressed directly by mesenchymal cells, cells having undergone EMT, cancer cells, senescent fibroblasts, and interestingly by cells bound and infected by the SARS virus (see Table 1). Exogenous sources of vimentin are largely related to immune response and tissue injury in the form of vimentin exported by neutrophils, T-lymphocytes, monocytes/macrophages, and exosomes. Schematics generated with Biorender.com.

Source	Description	Reference
Extracellular Sources – Largely implicated in immune and tissue injury		
Neutrophils	Released during apoptosis or NET formation; Source of serum citrullinated vimentin commonly found in rheumatoid arthritis	(*26, 34*)
Monocytes/Macrophages	Secreted after simulation by TNF-α or oxidized low density lipoprotein; possibly tissue injury; phosphorylated	(*27, 35*)
T-lymphocytes	Released on apoptosis; Binds phospholipase II to promote arachidonic acid metabolism	(*36*)
Exosomes	Astrocytes, activated by injury, can produce extracellular vimentin in the form of exosomes that are delivered to neurons; pre-adipocytes	(*37-39*)
Sources from the cell itself – Mesenchymal and transformed cells		
Mesenchymal cells/EMT	Vimentin is expressed endogenously in mesenchymal cells and is a wide-spread marker EMT	(*40, 41*)
Cancer	Intracellular: Upregulation of vimentin in multiple types of cancer; Extracellular: Target for isolating circulating tumor cells, designing vaccines and enhanced chemotherapy; sometimes proteolyzed	(*42, 43*)
Senescent Fibroblasts	Post-translational modification of cysteine 328 by malondialdehyde in senescent cells leads to its secretion and surface exposure	(*44*)
SARS Stimulation	Extracellular vimentin expression increases upon SARS binding to cell surface; SARS-CoV also upregulates cytoplasmic vimentin by the TGF-β pathway to promote a fibrotic response in lung cells	(*19, 45*)

Table 1. Sources of intracellular and exported vimentin

b. Binding of vimentin to the SARS-CoV-2 spike2 protein.

Next, we tested whether vimentin could bind to manufactured virus-like particles (VLPs) coated in SARS-CoV-2 spike protein in vitro. Binding of purified bacterially-expressed human vimentin to these VLPs was measured by a combination of dynamic light scattering (DLS) and imaging by atomic force microscopy (AFM). Figure 2A shows that the hydrodynamic radius of the pseudovirus was 60 nm, consistent with the expected size of the virus diameter of 120 nm and similar to the size of SARS-CoV-2 (*46*). As purified vimentin was added to the VLP, its hydrodynamic radius increases to approximately 150 nm. The increase in apparent size is not due to a separate contribution of large vimentin filaments to the mixture, because scattering from vimentin alone was negligible at all concentrations compared to that of the VLP, and the increase in scattering of the mixtures is larger than the sum of separate contributions from VLP and vimentin (SI Fig.1). Separate measurement of the vimentin used for these studies showed that its effective hydrodynamic diameter was 150 nm, which represents small

oligomers of vimentin similar in size to those reported at the cell surface (*47*). An estimate of the stoichiometry of vimentin oligomers to spike proteins is made from the

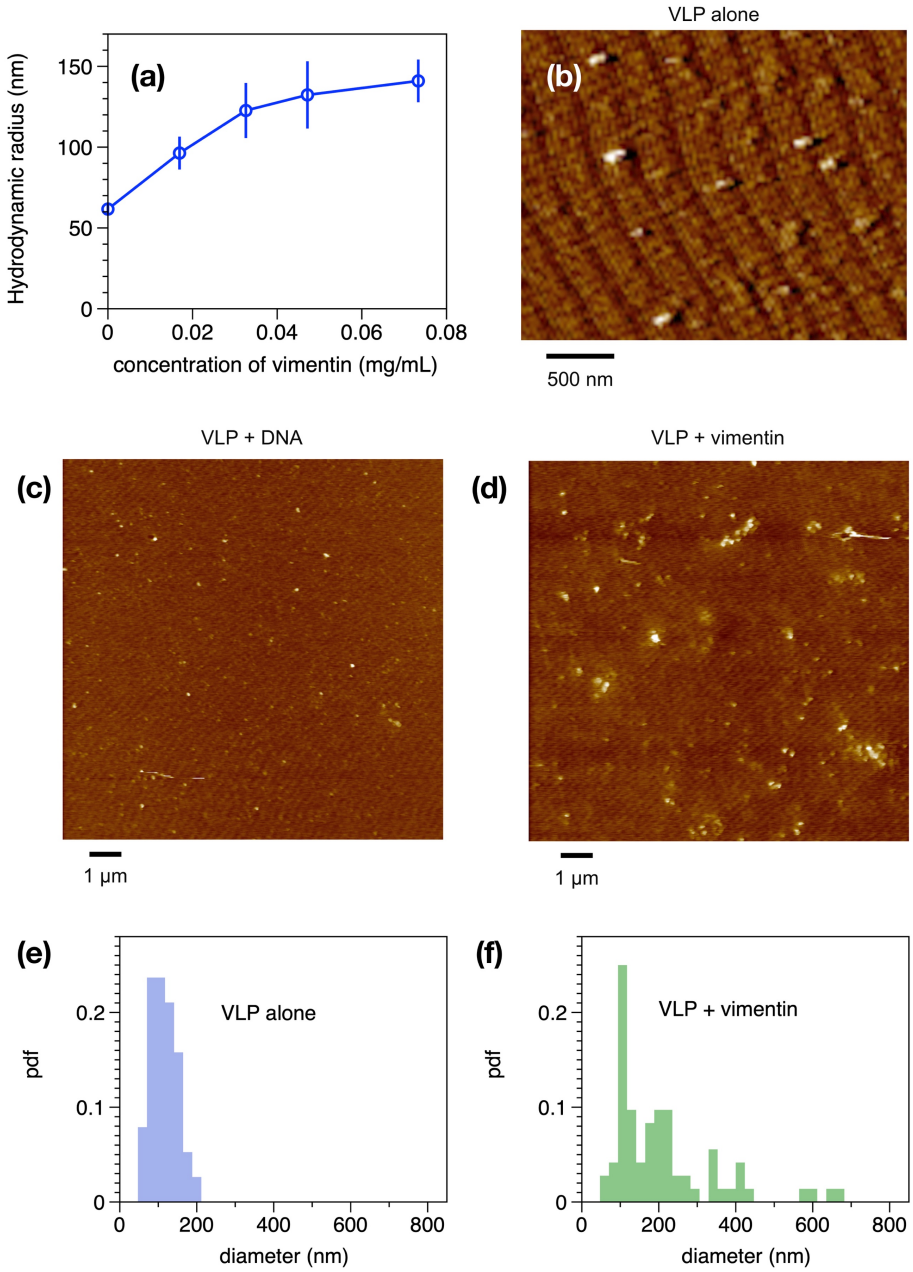

Figure 2. Binding of vimentin to SARS CoV-2 pseudovirus. Purified human recombinant vimentin was added to suspensions of SARS-CoV-2 spike protein-containing pseudovirus, and their size was measured by dynamic light scattering (a) and atomic force microscopy (b-f). The size of the viral particles increased from 60 nm to 150 nm after addition of 0.07 mg/ml vimentin. Panels b-d show that the effect of vimentin on the pseudovirus was specific for vimentin because double stranded DNA polymers with similar size and surface charge did not affect the virus size. The pseudovirus was imaged by atomic force microscopy before (e) an after (f) addition of 0.07 mg/ml vimentin. The probability distribution functions (pdfs) show that the average size of viral particles imaged by AFM confirms the change in size detected by DLS.

concentration of VLPs given by the manufacturer as 10^9/mL, and the weight concentration and size of vimentin oligomers. Estimating the vimentin oligomer length as the hydrodynamic diameter, and the length of a vimentin unit length filament as 65 nm, leads to an estimate of 3 x 10^{12} vimentin oligomers/mL at the highest concentration. Assuming each VLP contains 50 spike proteins leads to an estimate of 5 x 10^{10} spike proteins/mL. Therefore at the highest concentration in the titration, there is a 60x excess of vimentin oligomers to spike protein. Binding of vimentin oligomers or short filaments to the VLP was selective for vimentin; we found that similar increases in VLP size after titration with three different preparations of vimentin, but no significant increase after addition of double stranded DNA, a polymer that is also found extracellularly with similar size and surface charge (data not shown).

The samples used for DLS were also examined by atomic force microscopy. Figure 2 shows the VLPs alone (Fig 2b) and VLPs after addition of DNA (Fig. 2c) or vimentin (Fig. 2d). Histograms of the size distributions (Figures 2e and f) show VLP diameters consistent with the radii measured by DLS and that after addition of vimentin, some single VLPs appear larger, but small clusters of VLPs, presumably bridged by vimentin oligomers are common. Overall, the data in Figure 2 shows that purified vimentin can bind the SARS-CoV-2 spike protein-containing VLP and cause it to aggregate, but that other anionic biopolymers such as DNA have no effect on the VLP (SI Fig. 2).

c. Anti-vimentin antibodies block uptake of SARS-COV-2 virus-like particles in cultured human epithelial cell lines

If extracellular vimentin can bind to SARS-CoV-2 virus and help capture it at the cell surface, then vimentin might increase SARS-CoV-2 host cell invasion, and anti-vimentin antibodies could block its uptake. To test this idea, we identified two model cell lines, human embryonic kidney epithelial cells HEK 293T-hsACE2 (Figure 3), which stably express ACE2 to enable host cell invasion by the SARS-CoV-2 virus or virus-like particles. Both of these epithelial cell lines express vimentin, though the presence of cell surface vimentin was unclear. Thus, we performed immunofluorescence studies comparing cells treated with primary anti-vimentin antibodies before fixation versus after fixation and cell membrane permeabilization by Triton X-100 (Methods). We compared our results with mouse embryonic fibroblasts that form intracellular filamentous vimentin networks, emblematic of mesenchymal cells (Fig. 4a). The presence of cell surface vimentin was detected on HEK 293T-hsACE2.

Next, host cell invasion studies were conducted using SARS-CoV-2 virus-like particles bearing a green fluorescent protein (GFP) plasmid reporter. Cultured cells were exposed to varying dilutions of VLPs concentration (Methods), and the resulting number of infected cells was detected by epifluorescence microscopy of cell GFP expression and monitored over the course of three days. As expected, the number of GFP-

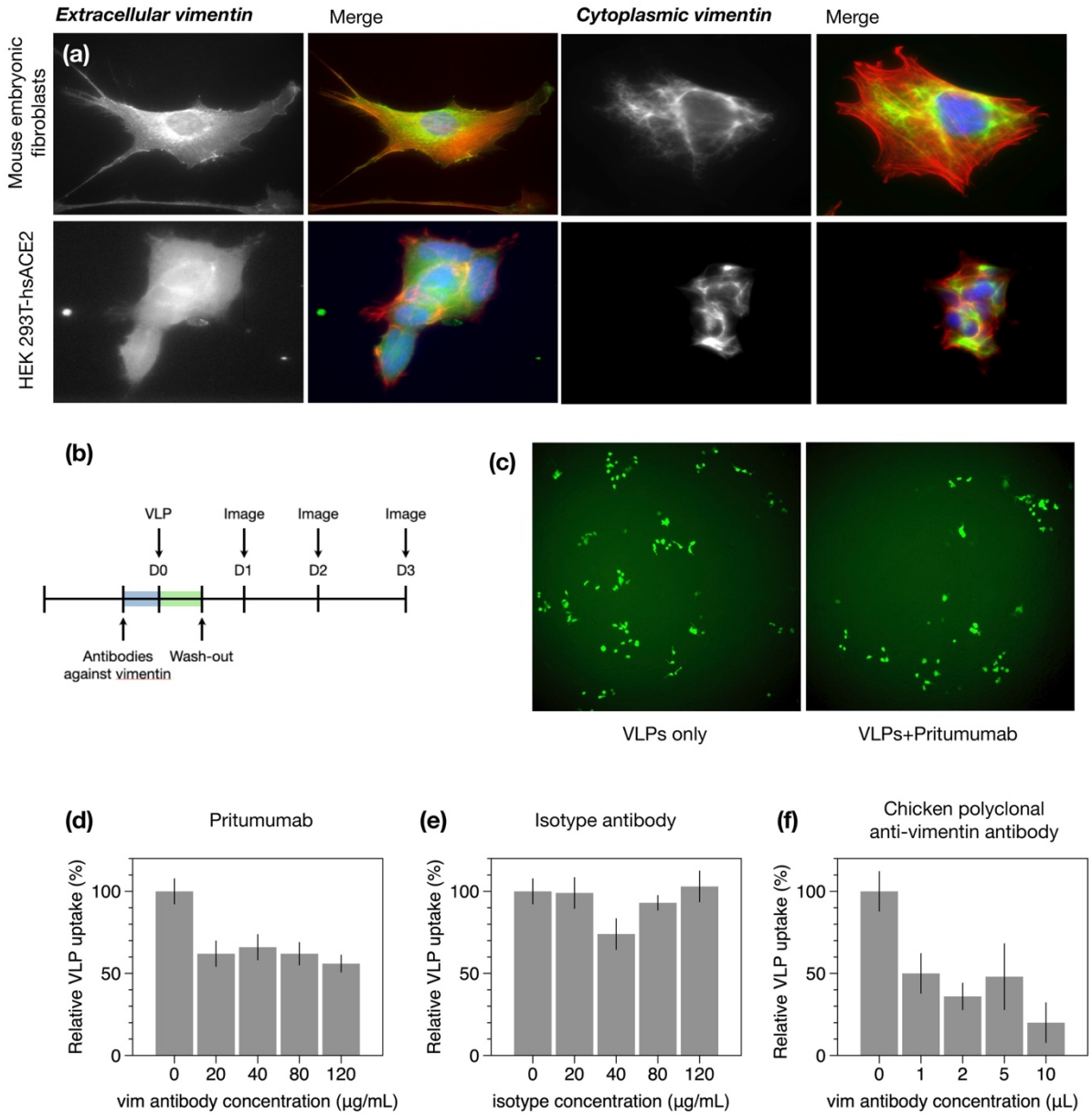

Figure 3. Anti-vimentin antibodies block uptake of SARS-CoV-2 virus-like particles in HEK 293T-hsACE2. (a) Positive staining for extracellular vimentin in mouse embryonic fibroblasts and human kidney epithelial cells HEK 293T-hs ACE2 and mouse embryonic fibroblasts. Images show vimentin (green), actin (red), and DNA (blue). To stain for extracellular vimentin, cells were exposed to a primary polyclonal chicken anti-vimentin antibody, before fixation, then permeabilized and stained for actin. (**b)** Schematic of experimental design of VLP infection studies. HEK cells are pre-exposed to the anti-vimentin antibody Pritumumab before infection by virus-like particles (VLPs) bearing the SARS-CoV-2 spike protein and a GFP reporter. **(c)** Representative fluorescence images showing cells expressing GFP after VLP exposure with and without Pritumumab treatment. **(d)** Pritumumab inhibits cellular infection by up to 60%. **(e)** Use of an isotype antibody does not inhibit infection, corroborating a specific interaction between the SARS-CoV-2 spike protein and extracellular vimentin. **(f)** Use of another vimentin antibody, a chicken IgY polyclonal antibody, also blocks cellular infection by SARS-CoV-2 VLP.

expressing cells reached a maximum three days after VLP exposure and was VLP load dependent. Maximum infection rates were in the range of 1 to 10% among experimental replicates for HEK 293T-hsACE2.

Can anti-vimentin antibodies block SARS-CoV-2 uptake and does inhibition depend on the antibody's vimentin-binding epitope? To address this question, we presented cells with a number of different antibodies against vimentin (see Table 1) and measured the resultant change in infection compared to the case without antibodies. We began these studies with perhaps the most promising therapeutic anti-vimentin antibody, Pritumumab, a human-derived IgG antibody, reported to be specific against extracellular vimentin and known to bind to vimentin's C-terminal domain (*48*). In this case, we pre-exposed HEK 293T-hsACE2 cells with various concentrations of Pritumumab prior to infection by SARS-CoV-2 VLP and found a dose-dependent decrease in infection efficiency. We found a maximum reduction of VLP infection of up to 60% when cells were incubated with 120 µg/ml Pritumumab (Fig. 3d). The specificity of the Pritumumab interaction with extracellular vimentin was tested against an IgG isotype antibody control (Fig. 3e), which did not block uptake of the SARS-CoV-2 VLP, suggesting a specific interaction between vimentin and the SARS-CoV-2 spike protein.

Next, we tested the efficiency of other anti-vimentin antibodies (Table 2) in blocking host cell invasion by SARS-CoV-2 VLPs and sought a vimentin binding domain that could be targeted against SARS-CoV-2 (Table 2). We used: (i) a chicken polyclonal antibody that binds to multiple epitopes; (ii) anti-vimentin antibodies targeting parts of the C terminus: in addition to Pritumumab, a human vimentin IgG against amino acid 300; and (iii) antibodies against the N-terminus: a rabbit monoclonal antibody corresponding to residues surrounding Arg45 and a polyclonal rabbit antibody IgG around the non-phosphorylation site of Ser56.

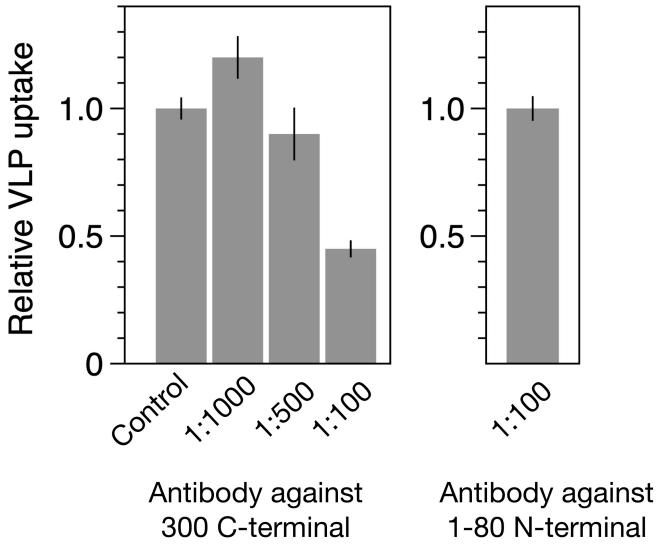

Figure 4. SARS-CoV-2 VLP infection results from plate readers. The recombinant Anti-Vimentin antibody – rabbit monoclonal IgG, which binds to the vimentin C-terminus blocks uptake in HEK 293T-hsACE2. The primary anti-vimentin polyclonal rabbit antibody that targets the phosphorylation site of SER56 on the N-terminus blocks uptake does not block uptake in HEK 293T-hsACE2 cells.

Some but not all anti-vimentin antibodies blocked SARS-CoV-2 VLP cellular uptake in a dose-dependent manner. Using epifluorescence microscopy to detect SARS VLP infection in HEK 293T-hsACE cells, we found that the polyclonal antibody against vimentin decreased host cell

invasion by up to 80% (Fig. 3f), whereas the rabbit monoclonal antibody targeting the N-terminal was not effective at blocking uptake (SI Fig. 3). As an independent measurement, we used plate readers to measure GFP expression due to SARS-CoV-2 VLP infections (Fig. 4). In this case, the recombinant antibody against the C-terminal 41- amino acids and the polyclonal rabbit antibody targeting Ser56 of the vimentin N-terminal were used. The C-terminal antibody was efficient in blocking uptake up 60%. The Ser56 antibody did not block uptake. Taken together, our results suggest that antibodies targeting the C-terminal tail domain of vimentin are most efficient in blocking SARS-CoV-2 host cell invasion, whereas antibodies against the N-terminus were generally not.

Anti-Vimentin antibody	**Binding domain on vimentin**	**Effectiveness in blocking uptake of SARS-CoV-2 VLP**
Pritumumab (Nascent Biotech); A natural human IgG1 kappa antibody was obtained from a regional draining lymph node of a patient with cervical carcinoma	Epitope is the C2 core region (coil 2 of the central rod) of cell-surface vimentin (*48, 49*)	Blocks uptake in HEK 293t-hsACE2 up to 60%
Chicken polyclonal IgY antibody (Novus Biologicals)- Cat# NB300-223	Polyclonal antibody, multiple epitopes	Blocks uptake in HEK 293t-hsACE2 up to 80%
Rabbit Monoclonal (Cell signaling Technology) Cat# #5471	N-terminal; produced by immunizing with a synthetic peptide corresponding to residues surrounding Arg45 of human vimentin	Does not block uptake in HEK 293t-hsACE2
Recombinant Anti-Vimentin antibody – IgG MW~150kDa [EPR3776] (Abcam) Cat# ab92547	C-terminal; produced by immunizing with a synthetic peptide containing 17 residues from within amino acids 425-466 of human vimentin	Blocks uptake in HEK 293T-hsACE2 by 60%
Primary anti-vimentin polyclonal rabbit antibody IgG ~150kDa (antibodies-online.com) Cat# ABIN6280132	N-terminal; Synthesized peptide derived from human Vimentin around the non-phosphorylated site of Ser56, Binding Specificity AA 1-80, Ser56	Does not block in HEK 293T hsACE2

Table 2. List of anti-vimentin antibodies

d. Cell surface vimentin acquisition from the extracellular environment.

Our results thus far suggest that extracellular vimentin might bind to the SARS-CoV-2 spike protein and enhances host cell invasion by the SARS-CoV-2 virus. Studies on SARS and SARS-CoV-2 indicate that while ACE2 is required for infection, it is not solely sufficient for cellular uptake and invasion (7). We therefore posit that extracellular vimentin is a key player in SARS-CoV-2 invasion and that its presence in the lung and other tissues is an important pre-condition of the extracellular environment that enhances SARS-CoV-2 infection. As a pre-requisite, we have identified that vimentin is present in extracellular space of healthy adult lung and fat tissue (Fig. 1). Vimentin may appear on the cell surface and in the extracellular space of the lung via numerous routes (Fig. 1, Table 1). These routes are likely associated with inflammatory response in the course of disease (e.g. fibrosis and cancer) but might also reflect homeostatic regulation associated with normal tissue functions and maintenance. In the context of the lung, the most probable sources are vimentin-expressing lymphocytes, macrophages and neutrophils that specialize in fighting off pathogens.

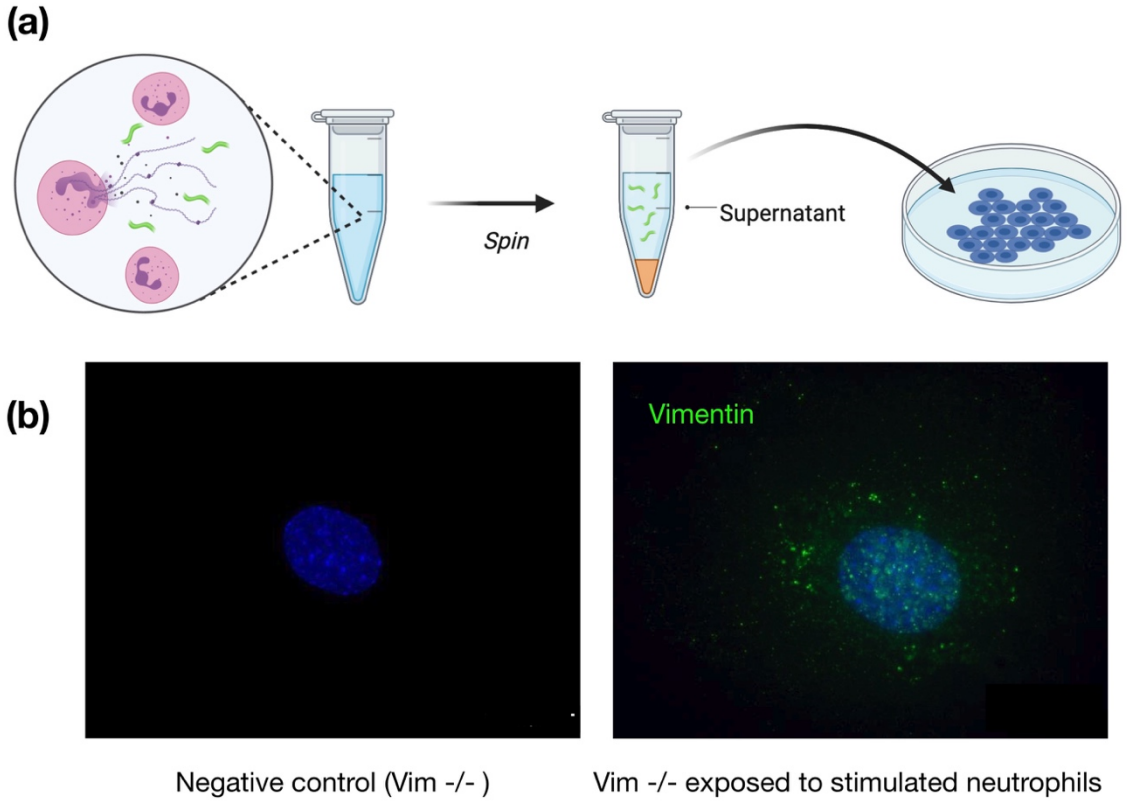

Figure 5. Acquisition of cell surface vimentin from extracellular environment. (a) Neutrophil NETosis stimulates disassembly of the vimentin network and enables its release into the extracellular space. **(b)** Immunofluorescence images of vimentin-null mEF staining positive for extracellular vimentin after exposure to supernatant of NETosis-activated neutrophils, indicating the acquisition of extracellular vimentin by cells that do not express vimentin. Schematics generated with Biorender.com.

Here, we demonstrate a novel mechanism by which non-vimentin expressing cells acquire cell surface vimentin from the extracellular environment via neutrophil NETosis (*25, 34*). NETosis represents one of the mechanisms of host defense, in which neutrophils expel large webs of DNA that entrap bacteria. Additionally, during NETosis disassembly of the vimentin network take place. NETosis requires activation of peptidyl arginine deiminase 4 (PAD4), which citrullinates histones in the process of releasing DNA from neutrophil heterochromatin. At the same time, the cytoskeleton disassembles to allow the nuclear content released after nuclear membrane rupture to reach the plasma membrane and eventually enter the extracellular space as the plasma membrane ruptures (*34*). Disassembly of the vimentin network is also promoted by citrullination, and vimentin is a major substrate for PADs (*25*). Citrullination leads to disassembly of the vimentin network, which can then be released into the extracellular space and become accessible to the cell surfaces of other tissues.

To show that neutrophil-released vimentin can be acquired on the surface of other cell types, we stimulated NETosis in neutrophils with phorbol myristate acetate (PMA), collected the supernatant following centrifugation, and then incubated the supernatant with a different cell type (Fig. 5a). Here we used vimentin-null mouse embryo fibroblasts (mEF), so that any vimentin detected on their surface was indicative of vimentin acquired from the extracellular environments. As shown in Fig. 5b, after exposing cells to the supernatant containing NETs (positive for DNA and elastase; data not shown), the vimentin-null cells stained positive for cell-surface vimentin in immunofluorescence microscopy. Taken together, these results highlight that NETosis leads to release of vimentin to the extracellular environment, highlighting a new avenue by which vimentin is deposited on the extracellular surface of cells and the extracellular space of tissue.

e. Possible role of cell surface vimentin in endocytosis.

Our results thus far indicate that extracellular vimentin binds to the SARS-CoV-2 spike protein and facilitates host cell invasion by SARS-CoV-2 VLP, which suggests that extracellular vimentin might acts as a co-receptor for the SARS-CoV-2virus. Host cell entry of SSARS-CoV-2 is not fully characterized, but inhibition of both fusion (*50*) and endocytosis (*51*) and are known to prevent viral invasion. Typical endocytic pathways include clathrin-mediated endocytosis, caveolin-mediated endocytosis, and macropinocytosis (*52*) (*53-55*). If extracellular vimentin traps the SARS-CoV-2 virus at the cell membrane, it might therefore alter viral invasion by either membrane fusion or endocytic pathways.

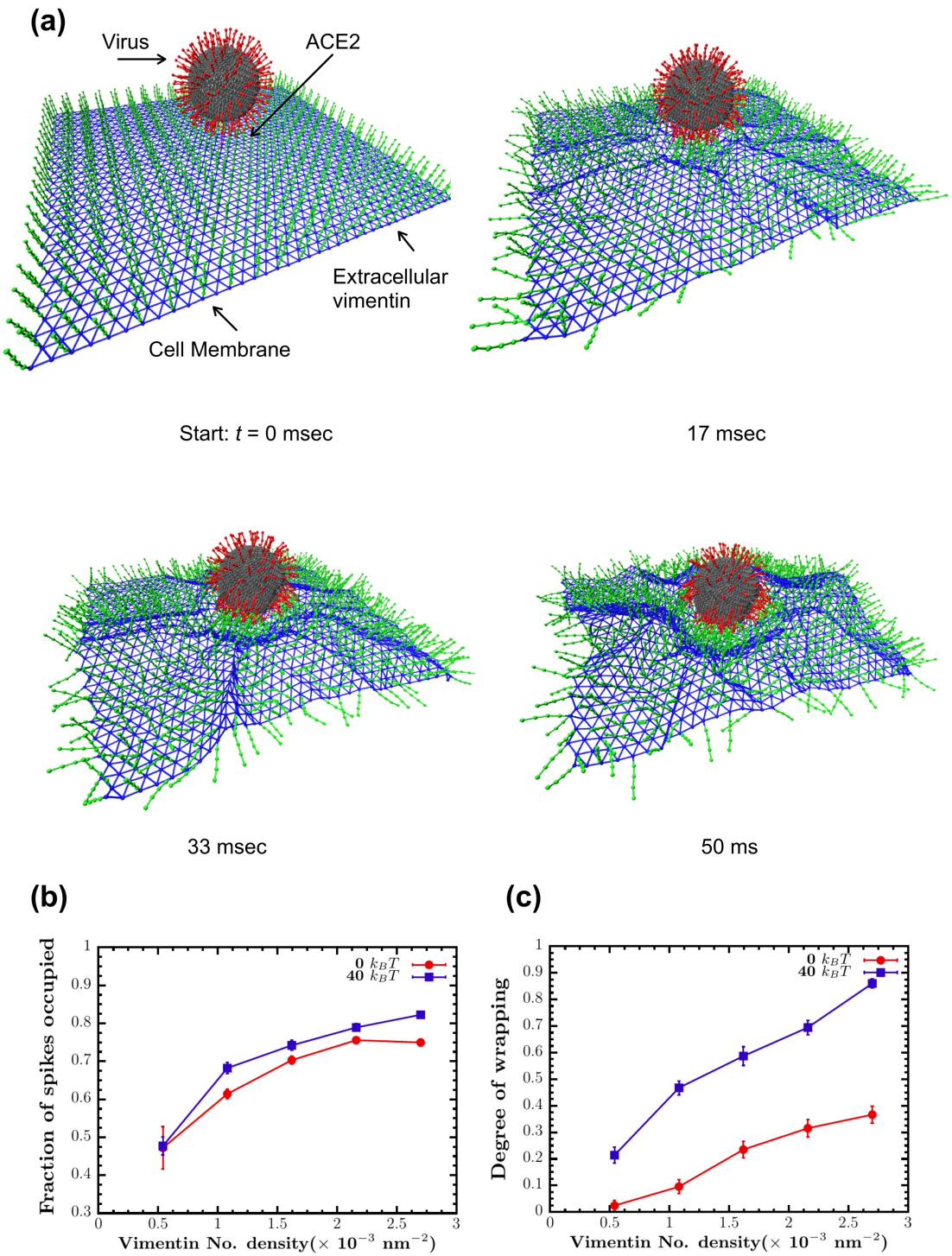

Figure 6. Vimentin's involvement in spike 2-ACE2 interactions. (a) Cell surface vimentin acts as a co-receptor that enhances binding to the SARS-CoV-2 virus in either direct fusion or endocytic pathways to enhance wrapping and endocytosis of the virus. A molecular dynamics simulation of the SARS-CoV-2 virus at an elastic shell membrane shows that binding of extracellular vimentin with the virus spike protein facilitates wrapping of cell membrane around the virus. Both the fraction of spikes bound to surface vimentin **(b)** and the degree of membrane wrapping **(c)** increases as the number density of surface vimentin increases. Finite membrane bending rigidity (40 k_BT, blue squares) enhances wrapping compared to the case without bending rigidity (0 k_BT, red circles).

In terms of membrane fusion, the SARS-CoV-2 virus uses a similar pathway as SARS, employing the ACE2 receptor and the transmembrane protease serine 2 TMPRSS2 (*50*) to invade cells. Assuming extracellular vimentin is bound to the cell membrane, it could help stabilize virus-cell membrane docking and mediate membrane leaflet separation for membrane fusion, depending on the detailed coupling between vimentin and the SARS-CoV-2 virus and whether extracellular vimentin alters the cell membrane properties. In terms of endocytosis, the SARS virus is known to use clathrin-dependent entry (*55*), but much less is known for SARS-CoV-2. Our immunofluorescence imaging indicated that extracellular vimentin appears in patches on the cell surface, at length scales of at least several virus diameters (Fig.3). We thus presume that vimentin might initiate endocytic wrapping of the cell membrane around the virus, just as clathrin does from within the cell (*53-55*): vimentin and clathrin would generate opposite membrane curvatures, working together to wrap the membrane from both sides.

To test this idea, we conducted a 3D computational model simulating the interactions among the SARS-CoV-2 virus, extracellular vimentin, and the surface of the cell membrane. The virus is modeled as a deformable sphere with 200 spikes, using an upper bound on spike protein containing binding sites (*56*). The cell membrane is modeled as an elastic sheet. To study the effect of the bending rigidity of the cell membrane on this process, we model the case of a purely elastic membrane with no bending rigidity (0 k_BT) versus one with finite membrane rigidity (40 k_BT). The cell-surface vimentin is bound to the membrane and is modeled as semiflexible polymers of length 40 nm, motivated by recent work that shows extracellular vimentin is mainly in the form of oligomers with 4-12 monomers and tetramers, but is not filamentous (*47*). The cell surface vimentin is bound to the cell membrane and can bind to the spike protein. For modeling details, see Methods and SI materials.

Using this model, we quantify how cell surface vimentin initiates endocytosis of SARS2 as a function of cell surface vimentin coverage, or the fraction of membrane nodes with bound cell surface vimentin (Fig. 6). We find that as cell surface vimentin coverage increases the fraction of spikes bound to cell surface vimentin increases from approximately 0.45 to 0.8, pointing to enhanced interactions between the two. Increasing cell surface vimentin also enhances the degree of membrane wrapping around the cell virus, which we define here as a metric of cell membrane curvature in the vicinity of the virus (Methods). Interestingly, finite cell membrane bending rigidity enhances wrapping of the virus, as compared to the case where the cell membrane is purely elastic. This result suggests that spatial correlations of the cell membrane via bending enhance the likelihood of endocytic initiation of SARS-CoV-2 via cell surface vimentin. Taken together, these numerical studies indicate a wide range of condition in which cell surface vimentin may aid in SARS-CoV-2 host cell invasion.

III. Discussion

Identifying targets against SARS-CoV-2 is critical because evidence suggests that viral load is correlated to the severity of COVID-19 infection in patients *(57)*. Here, we have shown that extracellular vimentin promotes SARS-CoV-2 uptake in lung and kidney epithelial cells and antibodies targeted against vimentin block it (Fig. 7). Thus, we propose that vimentin-blocking antibodies could serve as a promising therapeutic strategy against SARS-CoV-2 and future coronaviruses, decreasing viral load, and subsequent patient symptoms.

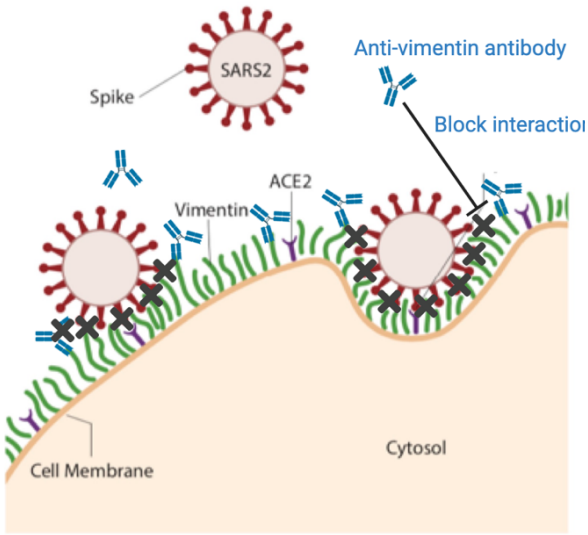

Figure 7. Extracellular vimentin as a potential target for inhibiting SARS-CoV-2 entry. A diagram of proposed mechanism of action. Here, cell surface vimentin (green) acts as a co-receptor that binds to SARS-CoV-2 spike protein. Blocking this interaction via the anti-vimentin antibody Pritumumab reduces cell surface binding of the virus and cellular infection. Schematics generated with Biorender.com.

Although generally considered primarily an intracellular, cytoskeleton protein, a large body of evidence shows that vimentin can also be found on the external surface of cells and in extracellular fluids. Numerous pathways have been identified for controlled release of vimentin often by inflammatory cells. Extracellular release depends on covalent modifications of vimentin, often by phosphorylation or citrullination (*30*). These modifications disassemble cytoskeletal vimentin intermediate filaments and lead to release of vimentin either on the external surface of the same cell or in soluble form or on the surface of exosomes where it can target cells such as epithelial cells (*58*) or neurons (*38, 39*) that do not express vimentin endogenously. Cell surface vimentin is reported to function normally during some types of wound healing (*39, 58, 59*) but is also often increased during pathological states such as cancer (*60, 61*). Numerous pathogens, both viruses and bacteria, exploit cell surface vimentin to gain entry to the host cell (*11-19*). In bacteria, engagement of vimentin is often due to binding of essential virulence factors (*62*). For viruses that are affected by vimentin, binding depends on coat proteins, and for SARS, the ligand for vimentin is its spike protein, which is similar to the spike proteins of SARS-CoV-2 (*19*).

There are two main pathways by which the SARS-CoV-2 virus is thought to attach and bind to cells for infection. The first is through the transmission of respiratory droplets that enter and move through the nasal and lung epithelial airways. The second way occurs after initial infection by entering into the bloodstream, where it can enter

endothelial cells and lead to inflammation and damage in organs such as the heart, kidney, and liver. Thus, our results suggest two general therapeutic strategies to prevent and reduce SARS-CoV-2 infections. The first is to aerosolize the antibody and use it as a nasal spray as a preventive measure against SARS-CoV-2 infection, and the second is intravenously, alone or in combination with other viral inhibitors, to reduce further uptake and subsequent inflammation.

The utility of an initial binding event at the cell surface prior to engagement of the viral spike protein by its receptor ACE2 is supported by the binding kinetics of the spike protein from SARS or SARS-CoV-2 to an immobilized chimera of the ACE2 extracellular domain and the Fc fragment of IgG. Surface plasmon resonance measurements show that although the affinity of the SARS-CoV-2 spike protein is greater than that of SARS spike protein, the rate of binding is much slower (*1, 6*). Therefore, engagement of the virus by an ACE2 bearing cell would be highly enhanced if the virus was first immobilized by a faster binding event. While the kinetic binding rates between vimentin and the SARS-CoV-2 spike protein have yet to be measured, it is likely much faster than the slow binding time between SARS-CoV-2 spike protein and the ACE2 receptor. Thus, extracellular vimentin would serve as a critical co-receptor, binding and engaging with the SARS-CoV-2 virus at the surface of the cell membrane, enhancing its delivery to the ACE2 receptor.

Finally, while these studies focus on the critical first few steps by which SARS-CoV-2 infects cells, there are *in vitro* and *in vivo* studies that suggest an active role of extracellular vimentin post-infection by SARS and SARS-CoV-2. For instance, a recent study using Vero E6 cells showed that cell surface vimentin levels increased over 15% after exposure to SARS-CoV VLP (*19*). Interestingly, another study of over 80 patients with respiratory failure secondary to severe SARS-CoV-2 pneumonia found extracellular vimentin in the bronchoalveolar lavage (BAL) fluid of infected patients (*63*). Vimentin appears to have a complicated role in pathogenesis, acting as both a target for infection (*19, 64, 65*) and an important actor for proper immune response (*25, 27, 66*). Our results here suggest that extracellular vimentin acts as a novel target for SARS-CoV-2 entry inhibition. Identifying the mechanisms that lead to the expression, trafficking, and secretion of vimentin will be pivotal to mediating its role in tissue damage and repair during viral infections.

IV. Conclusions

Vimentin is secreted into the extracellular environment by multiple cell types and its presence can provide positive signals for wound healing and act as a cofactor for pathogen infection. Both monoclonal anti-vimentin antibodies and a vimentin-specific DNA aptamer developed to isolate circulating cancer cells (*67*) are being applied to infection by SARS-CoV (*19*) and other viruses (*68*). Here, we have demonstrated a new role of extracellular vimentin in SARS-CoV-2 host cell invasion. Further, we find that antibodies against vimentin can block up to 80% of host cell invasion *in vitro*. Our

results suggest a new target and therapeutic strategy to reduce SARS-CoV-2 attachment and entry into the cell, which could reduce the spread of the SARS-CoV-2 virus and other possible pathogens.

V. Methods

Cell culture. In this study five cell lines were used: wild-type mouse embryonic fibroblasts (mEF vim +/+), vimentin-null fibroblast (mEF vim -/-), and human kidney epithelial cells HEK293T ACE2-transfected (Integral Molecular, Integral Cat# C-HA101). Cells were cultured in DMEM (ATCC) with 10% of fetal bovine serum (FBS), penicillin (50 µg/mL) and streptomycin (50 µg/mL). Kidney derived cells were additionally treated with 0.5 µg/mL puromycin to maintain ACE2 receptor expression. Cells were maintained at 37°C in an atmosphere containing 5% CO_2 with saturated humidity.

Tissue staining. To evaluate presence of extracellular vimentin on the surface of cells within human tissue, fluorescent immunohistochemistry staining was performed. To do so, paraffin-embedded human lung and fat tissue, as well as sputum obtained from cystic fibrosis patients were cut into 15 µm thick slices on a rotary microtome and placed on glass slides. After overnight drying, slides were rehydrated by immersion in xylene and ethanol for 10 min at each step. Slides were hydrated with PBS and transferred to EDTA-containing antigen retrieval solution (Sigma) for 1h at 100°C. Subsequently, samples were blocked in blocking buffer (1% BSA in PBS) for 30 min at RT. Primary rabbit anti-vimentin antibodies to the C-terminus at 1:200 were placed directly on tissues and left for overnight incubation in humidified chamber at 4°C. Afterwards, slides were washed three times for 15 min in PBS and incubated with secondary anti-rabbit Alexa Fluor 488-conjugated antibody at 1:500 for 1h at RT, protected from light. Following the washing step, tissues were counterstained with DAPI and mounted with anti-fade mounting medium (Sigma). Visualization was performed on Leica DM2000 fluorescent microscope

Dynamic light scattering. In these studies, recombinant human vimentin was kindly provided from Josef Käs and Jörg Schnauss (University of Leipzig) and by Karen Ridge (Northwestern Univ). VLP size (hydrodynamic radius) was determined by dynamic light scattering (DLS) using a DynaPro 99 instrument (*69*). The method measures the diffusion constant of the particles using the autocorrelation function of fluctuations in scattered light intensity. The radius R_h is calculated from the relation $D = {k_B T}/{6\pi\mu R_h}$, where D is the translational diffusion constant, k_B is the Boltzmann constant, T is the temperature, and μ is the solvent viscosity. To examine the interaction between the SARS-CoV-2 VLP and vimentin, we performed DLS measurements on VLP solutions with and without addition of human recombinant vimentin. As a control for non-specific binding, in some cases, addition of DNA was used to determine how polyelectrolyte polymers other than vimentin interact with the VLPs. Interaction of spike protein S

incorporated into VLPs' surface with vimentin oligomers would increase R_h either by adding to the surface of a single VLP or resulting in aggregate.

Atomic force microscopy. A Multimode ™ AFM with a Nanoscope IIIa controller (Veeco, Santa Barbara, CA) operated in contact mode was used to image VLPs before and after addition of vimentin or DNA. The cantilevers used were silicon nitride with a spring constant of 0.35 N/m (Veeco, Santa Barbara, CA). The AFM was calibrated using a 3D reference of 200 nm height and 10 μm pitch (Digital Instruments, Santa Barbara, CA). Deflection and height images were obtained with scan rates of 1 Hz with a resolution of 512 pixels/line. Briefly, for AFM evaluation of VLPs in control (non-vimentin addition) and samples preincubated with human recombinant vimentin, a 10 μl drop of VLPs or VLPs/vimentin was applied on cleaved mica (SPI Supplies, West Chester, PA) and analyzed in a dried environment.

Immunostaining of cell surface vimentin. To visualize surface vimentin, cells were fixed at approximately 50-70% confluency in 4% paraformaldehyde for 30 min at 37°C. Following fixation, to avoid non-specific binding cells were incubated with blocking-buffer (1% BSA in PBS) for 30 min at RT. After blocking, cells were incubated overnight at 4°C with primary rabbit monoclonal and polyclonal anti-vimentin antibodies at 1:500. Next, cells were incubated for 1h at RT with an Alexa Fluor 488-conjugated goat anti-rabbit secondary antibody at 1:1000. Counterstain was performed with DAPI nuclear stain. To differentiate surface vimentin from intracellular vimentin, additional staining was performed with addition of permeabilization step with 0.1% Triton X-100 in PBS for 15 minutes. Images were captured with a fixed-stage Zeiss Axio Examiner Z.1 microscope (Carl Zeiss Microscopy GmbH, Germany) and confocal scanning unit (Yokogawa CSU-X1, Yokogawa Electric Corporation, Japan).

Antibodies. For fluorescent imaging of vimentin and for experiments using anti-vimentin antibodies to block host cell infection by SARS-CoV-2 VLP, we used the following anti-vimentin antibodies: (i) Pritumumab (Nascent Biotech), a human derived IgG antibody that targets the C-terminus of vimentin; (ii) Chicken polyclonal IgY antibody (Novus Biologicals, Cat# NB300-223); (iii) primary anti-vimentin monoclonal antibody developed in rabbit immunized with a 17-residue synthetic peptide from a region within human vimentin amino acids 425-466 (Abcam, Cat# ab92547); (iv) Rabbit Monoclonal (Cell signaling Technology, Cat#5471); and (v) Ser56 N-terminus aa 1-80 (primary anti-vimentin polyclonal rabbit antibody; antibodies-online.com, Cat# ABIN6280132).

In vitro infection of cells by VLP. HEK 293T-hsACE2 cell lines were used as infection hosts for SARS-CoV-2 GFP-reporter pseudovirus (Integral Molecular, Integral Cat# RVP-701G). Cells were then seeded in 96-well plates at approximately 50% confluency. VLPs were introduced to cells by pipetting 50 μL (at 10^9 VLP/mL) into each well and in some cases by a serial 1/2 dilution of the VLP. To assess the involvement of vimentin during SARS-CoV-2 infection, anti-vimentin antibodies were introduced into the wells

either at the same time as the VLP or for a short incubation time prior to VLP exposure. VLP were either washed out after a 2 hr exposure time interval or were allowed to incubate with the cells throughout the remainder of the experiment. Cells were incubated for 72h at 37°C.

Measurement of VLP infection VLP infection was measured in one of two ways: the first is via epi-fluorescence microscopy and the second is by a microplate reader. In the first case, the percentage of cells infected by SARS-CoV-2 pseudovirus was quantified by calculating the ratio of cells expressing GFP to the total number of cells. Cells were imaged using a Nikon Eclipse Ti (Nikon Instruments) inverted microscope equipped with an Andor Technologies iXon em+ EMCCD camera (Andor Technologies). Cells were maintained at 37°C and 5% CO_2 using a Tokai Hit (Tokai-Hit) stage top incubator and imaged using a 10x objective Pan Fluor NA 0.3 (Nikon Instruments) at 24 hr, 48 hr, and 72 hr time points after VLP infections. In some cases, nuclei were stained using Hoechst prior to imaging to facilitate counting total cell numbers. The total number of cells and the number of cells expressing GFP were manually counted in randomly selected 65 µm by 65 µm imaging windows in ImageJ. The percentage of cells infected is calculated by taking the ratio of the number of cells expressing GFP to the total number of cells.

For studies using a microplate reader, after 72 hr supernatant was removed and cells were washed gently with PBS. 100 µl of PBS was added to each well and fluorescence was measured with Varioskan LuX microplate reader (ex= 480, em= 530). Data are presented as relative pseudovirus uptake compared to control. Background fluorescence (no VLP treated cells) constitute less than 10% for HEK 293T-hsACE2.

Endocytosis model. To examine the interaction between extracellular vimentin and the SARS-CoV-2 virus, we developed a coarse-grained molecular dynamics-based 3D model. The model consists of the cell membrane, extracellular vimentin, the angiotensin-converting enzyme 2 (ACE2) receptor, the SARS-CoV-2 virus, and the interactions between them. A portion of the cell membrane (approximately 500 nm x 500 nm in area) is modeled as a tethered membrane with a bending rigidity of $40k_BT$. Based on prior experiments (*47*), the extracellular vimentin is considered to be a 40 nm semiflexible filament, bound to the surface of the cell membrane. For simplicity, we have assumed that the SARS2 virus is fully bound to the ACE2 receptor: the spike-ACE2 interaction is given a stiff harmonic spring as ACE2 has a high affinity towards spike protein (*1*)**.** We designed the SARS-CoV-2 virus as a 100 nm diameter elastic viral spherical shell, and viral shell is decorated with 200 spikes (an upper bound estimate), each containing sticky sites that bind to extracellular vimentin through an attractive Lennard-Jones potential. For excluded volume interactions, we implement soft-core repulsion springs should any two particles begin to overlap. Each simulation is run for a total of 10^8 simulation units corresponding to 50 s. We defined a degree of membrane wrapping metric to reflect membrane curvature as a measure of the depth of the bowl

generated by the cell membrane. Specifically, we measure the distance between the height of the cell membrane (far from the bowl) versus the height of the deepest invagination of the membrane bowl: this value is then normalized by the total height of the SARS-CoV-2 virus, 120 nm. (See SI Materials for full details on the model.)

Vimentin acquisition by neutrophils. To assess whether vimentin may be acquired from extracellular environment, supernatant from phorbol myristate acetate (PMA) stimulated neutrophils were added to the vim-null mEF. To do so, blood was obtained from healthy volunteers (protocol number for human blood draw: R-I-002/231/2019) and neutrophils were isolated by gradient density separation with use of Polymorphprep. Isolated neutrophils were counted and transferred to Eppendorf tubes containing DMEM at concentration $6x10^5$ cells/mL. 100 nM of PMA was added to neutrophils for 30 min at 37°C. After incubation, cells were centrifuged and 100 µl of supernatant was added to a prewashed well with $1.5x10^4$ vim-null mEFs in a black 96-well glass bottom plate for 30 minutes. In the next step, cells were washed three times, fixed and immunofluorescently stained as described above.

Statistical methods. Data are presented as mean values ± SEM. Each experiment was performed a minimum of two times unless otherwise stated. The unpaired, two-tailed Student's t test at the 95% confidence interval was used to determine statistical significance. *, $P \leq 0.05$; **, $P < 0.01$; ***, $P < 0.001$; NS, $P > 0.05$.

Acknowledgements: We acknowledge Robert Goldman, Karen Ridge, Krzysztof Pyrc, and Nav Singh for insightful discussions. This work was supported by NSF MCB 2032861 award to A.P. and J.M.S., NIH GM136259 award to P.A.J., and the National Science Center of Poland: UMO-2020/01/0/NZ6/00082 awarded to R.B.

Author contributions: Author contributions: LS, MS, RB and AP performed and analyzed the SARS-CoV-2 virus-like particle infection studies. DG and DI contributed to VLP infection analysis. LS, MS, JR, NM, and AP performed extracellular vimentin staining. RB and PJ designed and ran the dynamic light scattering experiments. FB performed and analyzed the atomic force microscopy measurements. SG and JMS developed the endocytosis model and analysis. PJ, JMS, RB, MS, JR and AP wrote the manuscript. RB and AP initiated and oversaw the entire project.

References

1. D. Wrapp *et al.*, Cryo-EM structure of the 2019-nCoV spike in the prefusion conformation. *Science* **367**, 1260-1263 (2020).
2. A. C. Walls *et al.*, Structure, function, and antigenicity of the SARS-CoV-2 spike glycoprotein. *Cell*, (2020).
3. F. Hikmet *et al.*, The protein expression profile of ACE2 in human tissues. *Mol Syst Biol* **16**, e9610 (2020).
4. J. A. Aguiar *et al.*, Gene expression and in situ protein profiling of candidate SARS-CoV-2 receptors in human airway epithelial cells and lung tissue. *European Respiratory Journal* **56**, 2001123 (2020).
5. Y. J. Hou *et al.*, SARS-CoV-2 Reverse Genetics Reveals a Variable Infection Gradient in the Respiratory Tract. *Cell* **182**, 429-446.e414 (2020).
6. C. Lei *et al.*, Neutralization of SARS-CoV-2 spike pseudotyped virus by recombinant ACE2-Ig. *Nat Commun* **11**, 2070 (2020).
7. N. Z. Cuervo, N. Grandvaux, ACE2: Evidence of role as entry receptor for SARS-CoV-2 and implications in comorbidities. *Elife* **9**, e61390 (2020).
8. J. L. Daly *et al.*, Neuropilin-1 is a host factor for SARS-CoV-2 infection. *bioRxiv*, (2020).
9. T. M. Clausen *et al.*, SARS-CoV-2 infection depends on cellular heparan sulfate and ACE2. *Cell* **183**, 1043-1057. e1015 (2020).
10. M. A. Tortorici *et al.*, Structural basis for human coronavirus attachment to sialic acid receptors. *Nat Struct Mol Biol* **26**, 481-489 (2019).
11. C. S. Teo, J. J. Chu, Cellular vimentin regulates construction of dengue virus replication complexes through interaction with NS4A protein. *J Virol* **88**, 1897-1913 (2014).
12. J. Yang *et al.*, Superficial vimentin mediates DENV-2 infection of vascular endothelial cells. *Sci Rep* **6**, 38372 (2016).
13. X. B. Chang *et al.*, Annexin A2 binds to vimentin and contributes to porcine reproductive and respiratory syndrome virus multiplication. *Vet Res* **49**, 75 (2018).
14. W. W. Wang *et al.*, [The role of vimentin during PRRSV infection of Marc-145 cells]. *Bing Du Xue Bao* **27**, 456-461 (2011).
15. Z. J. Wang *et al.*, Vimentin modulates infectious porcine circovirus type 2 in PK-15 cells. *Virus Res* **243**, 110-118 (2018).
16. Q. Zhang, D. Yoo, PRRS virus receptors and their role for pathogenesis. *Vet Microbiol* **177**, 229-241 (2015).
17. P. Turkki, M. Laajala, M. Flodstrom-Tullberg, V. Marjomaki, Human Enterovirus Group B Viruses Rely on Vimentin Dynamics for Efficient Processing of Viral Nonstructural Proteins. *J Virol* **94**, (2020).
18. K. Kobayashi, S. Koike, Cellular receptors for enterovirus A71. *Journal of Biomedical Science* **27**, (2020).
19. Y. T. Yu *et al.*, Surface vimentin is critical for the cell entry of SARS-CoV. *J Biomed Sci* **23**, 14 (2016).

20. W. Sungnak *et al.*, SARS-CoV-2 entry factors are highly expressed in nasal epithelial cells together with innate immune genes. *Nature medicine* **26**, 681-687 (2020).
21. C. G. Ziegler *et al.*, SARS-CoV-2 receptor ACE2 is an interferon-stimulated gene in human airway epithelial cells and is detected in specific cell subsets across tissues. *Cell*, (2020).
22. M. Kasper, P. Stosiek, The expression of vimentin in epithelial cells from human nasal mucosa. *European Archives of Oto-Rhino-Laryngology* **248**, 53-56 (1990).
23. H. Herrmann, U. Aebi, Intermediate filaments: structure and assembly. *Cold Spring Harbor Perspectives in Biology* **8**, a018242 (2016).
24. Harvey Lodish *et al.*, *Molecular Cell Biology,*. (W.H. Freeman, New York, ed. 4, 2000).
25. R. Khandpur *et al.*, NETs are a source of citrullinated autoantigens and stimulate inflammatory responses in rheumatoid arthritis. *Sci Transl Med* **5**, 178ra140 (2013).
26. E. Moisan, D. Girard, Cell surface expression of intermediate filament proteins vimentin and lamin B1 in human neutrophil spontaneous apoptosis. *J Leukoc Biol* **79**, 489-498 (2006).
27. N. Mor-Vaknin, A. Punturieri, K. Sitwala, D. M. Markovitz, Vimentin is secreted by activated macrophages. *Nat Cell Biol* **5**, 59-63 (2003).
28. T. A. Fasipe *et al.*, Extracellular Vimentin/VWF (von Willebrand Factor) Interaction Contributes to VWF String Formation and Stroke Pathology. *Stroke* **49**, 2536-2540 (2018).
29. B. Xu *et al.*, The endothelial cell-specific antibody PAL-E identifies a secreted form of vimentin in the blood vasculature. *Mol Cell Biol* **24**, 9198-9206 (2004).
30. A. E. Patteson, A. Vahabikashi, R. D. Goldman, P. A. Janmey, Mechanical and Non-Mechanical Functions of Filamentous and Non-Filamentous Vimentin. *Bioessays* **42**, 2000078 (2020).
31. D. S. Fudge, S. Schorno, The Hagfish Gland Thread Cell: A Fiber-Producing Cell Involved in Predator Defense. *Cells* **5**, (2016).
32. F. Danielsson, M. K. Peterson, H. Caldeira Araujo, F. Lautenschlager, A. K. B. Gad, Vimentin Diversity in Health and Disease. *Cells* **7**, (2018).
33. Z. Kang *et al.*, Obesity is a potential risk factor contributing to clinical manifestations of COVID-19. *International Journal of Obesity* **44**, 2479-2485 (2020).
34. H. R. Thiam *et al.*, NETosis proceeds by cytoskeleton and endomembrane disassembly and PAD4-mediated chromatin decondensation and nuclear envelope rupture. *Proc Natl Acad Sci U S A*, (2020).
35. A. Garg *et al.*, Vimentin expressed on Mycobacterium tuberculosis-infected human monocytes is involved in binding to the NKp46 receptor. *J Immunol* **177**, 6192-6198 (2006).
36. D. Huet *et al.*, SC5 mAb represents a unique tool for the detection of extracellular vimentin as a specific marker of Sezary cells. *J Immunol* **176**, 652-659 (2006).
37. Z. Chen *et al.*, Cytoskeleton-centric protein transportation by exosomes transforms tumor-favorable macrophages. *Oncotarget* **7**, 67387-67402 (2016).
38. M. Shigyo, T. Kuboyama, Y. Sawai, M. Tada-Umezaki, C. Tohda, Extracellular vimentin interacts with insulin-like growth factor 1 receptor to promote axonal growth. *Scientific Reports* **5**, 12055 (2015).

39. M. Shigyo, C. Tohda, Extracellular vimentin is a novel axonal growth facilitator for functional recovery in spinal cord-injured mice. *Sci Rep* **6**, 28293 (2016).
40. E. D. Hay, The mesenchymal cell, its role in the embryo, and the remarkable signaling mechanisms that create it. *Developmental dynamics: an official publication of the American Association of Anatomists* **233**, 706-720 (2005).
41. J. P. Thiery, H. Acloque, R. Y. Huang, M. A. Nieto, Epithelial-mesenchymal transitions in development and disease. *cell* **139**, 871-890 (2009).
42. A. Satelli, S. Li, Vimentin in cancer and its potential as a molecular target for cancer therapy. *Cell Mol Life Sci* **68**, 3033-3046 (2011).
43. A. Satelli *et al.*, EMT circulating tumor cells detected by cell-surface vimentin are associated with prostate cancer progression. *Oncotarget* **8**, 49329-49337 (2017).
44. D. Frescas *et al.*, Senescent cells expose and secrete an oxidized form of membrane-bound vimentin as revealed by a natural polyreactive antibody. *Proc Natl Acad Sci U S A* **114**, E1668-E1677 (2017).
45. S. W. Li *et al.*, SARS coronavirus papain-like protease induces Egr-1-dependent up-regulation of TGF-beta1 via ROS/p38 MAPK/STAT3 pathway. *Sci Rep* **6**, 25754 (2016).
46. N. Zhu *et al.*, A novel coronavirus from patients with pneumonia in China, 2019. *New England Journal of Medicine*, (2020).
47. B. Hwang, H. Ise, Multimeric conformation of type III intermediate filaments but not the filamentous conformation exhibits high affinity to lipid bilayers. *Genes Cells*, (2020).
48. H. Hagiwara, Y. Aotsuka, Y. Yamamoto, J. Miyahara, Y. Mitoh, Determination of the antigen/epitope that is recognized by human monoclonal antibody CLN-IgG. *Human antibodies* **10**, 77-82 (2001).
49. I. Babic *et al.*, Pritumumab, the first therapeutic antibody for glioma patients. *Human antibodies* **26**, 95-101 (2018).
50. M. Hoffmann *et al.*, SARS-CoV-2 cell entry depends on ACE2 and TMPRSS2 and is blocked by a clinically proven protease inhibitor. *Cell*, (2020).
51. A. Bayati, R. Kumar, V. Francis, P. S. McPherson, SARS-CoV-2 uses clathrin-mediated endocytosis to gain access into cells. *bioRxiv*, 2020.2007.2013.201509 (2020).
52. S. Mayor, R. G. Parton, J. G. Donaldson, Clathrin-independent pathways of endocytosis. *Cold Spring Harbor perspectives in biology* **6**, a016758 (2014).
53. T. Zhang, R. Sknepnek, M. J. Bowick, J. M. Schwarz, On the modeling of endocytosis in yeast. *Biophys J* **108**, 508-519 (2015).
54. W. Kukulski, M. Schorb, M. Kaksonen, J. A. Briggs, Plasma membrane reshaping during endocytosis is revealed by time-resolved electron tomography. *Cell* **150**, 508-520 (2012).
55. Y. Inoue *et al.*, Clathrin-dependent entry of severe acute respiratory syndrome coronavirus into target cells expressing ACE2 with the cytoplasmic tail deleted. *J Virol* **81**, 8722-8729 (2007).
56. S. Klein *et al.*, SARS-CoV-2 structure and replication characterized by in situ cryo-electron tomography. *Nature Communications* **11**, 5885 (2020).
57. Y. Liu *et al.*, Viral dynamics in mild and severe cases of COVID-19. *The Lancet Infectious Diseases*, (2020).

58. J. L. Walker, B. M. Bleaken, A. R. Romisher, A. A. Alnwibit, A. S. Menko, In wound repair vimentin mediates the transition of mesenchymal leader cells to a myofibroblast phenotype. *Mol Biol Cell* **29**, 1555-1570 (2018).
59. F. W. Lam, Q. Da, B. Guillory, M. A. Cruz, Recombinant Human Vimentin Binds to P-Selectin and Blocks Neutrophil Capture and Rolling on Platelets and Endothelium. *J Immunol* **200**, 1718-1726 (2018).
60. I. S. Batth *et al.*, Cell Surface Vimentin Positive Circulating Tumor Cell-Based Relapse Prediction in a Long-Term Longitudinal Study of Post-Remission Neuroblastoma Patients. *International Journal of Cancer*, (2020).
61. H. Noh *et al.*, Cell surface vimentin-targeted monoclonal antibody 86C increases sensitivity to temozolomide in glioma stem cells. *Cancer Lett* **433**, 176-185 (2018).
62. S. H. Huang *et al.*, Vimentin, a Novel NF-kappaB Regulator, Is Required for Meningitic Escherichia coli K1-Induced Pathogen Invasion and PMN Transmigration across the Blood-Brain Barrier. *PLoS One* **11**, e0162641 (2016).
63. R. A. Grant *et al.*, Alveolitis in severe SARS-CoV-2 pneumonia is driven by self-sustaining circuits between infected alveolar macrophages and T cells. *bioRxiv*, 2020.2008.2005.238188 (2020).
64. E. E. Bastounis, Y. T. Yeh, J. A. Theriot, Matrix stiffness modulates infection of endothelial cells by Listeria monocytogenes via expression of cell surface vimentin. *Mol Biol Cell* **29**, 1571-1589 (2018).
65. N. Du *et al.*, Cell surface vimentin is an attachment receptor for enterovirus 71. *J Virol* **88**, 5816-5833 (2014).
66. E. Boilard, S. G. Bourgoin, C. Bernatchez, M. E. Surette, Identification of an autoantigen on the surface of apoptotic human T cells as a new protein interacting with inflammatory group IIA phospholipase A2. *Blood* **102**, 2901-2909 (2003).
67. Y. Zheng *et al.*, Selection of Aptamers Against Vimentin for Isolation and Release of Circulating Tumor Cells Undergoing Epithelial Mesenchymal Transition. *Anal Chem*, (2020).
68. S. Das, V. Ravi, A. Desai, Japanese encephalitis virus interacts with vimentin to facilitate its entry into porcine kidney cell line. *Virus Res* **160**, 404-408 (2011).
69. N. C. Santos, A. C. Silva, M. A. Castanho, J. Martins-Silva, C. Saldanha, Evaluation of lipopolysaccharide aggregation by light scattering spectroscopy. *Chembiochem* **4**, 96-100 (2003).

Supplementary Figures

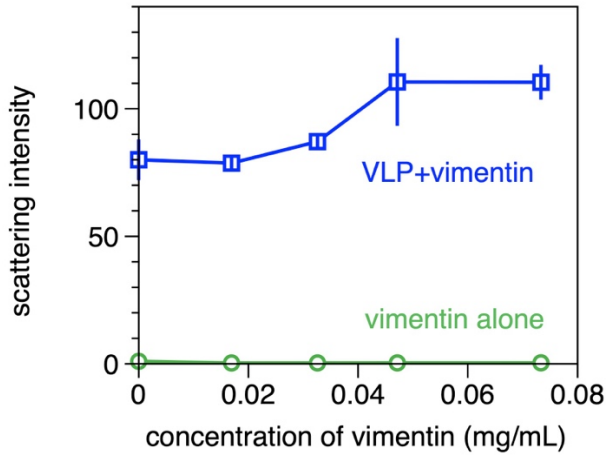

SI Fig. 1. The scattering intensity of the viral parties was much larger than that of the added vimentin (B) and was slightly increased after adding vimentin.

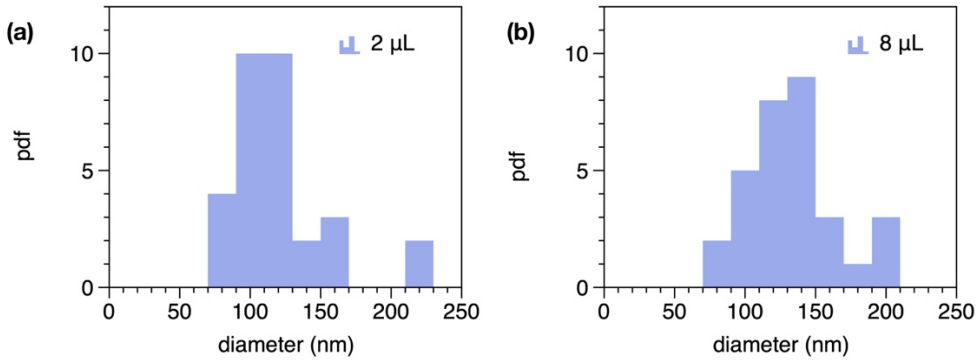

SI Fig. 2. The probability distribution function of particle diameter for SARS-CoV-2 VLP samples after the addition of either (a) 2 μL or (b) 8 μL of 10 mg/mL DNA. Particle sizes were measured by atomic force microscopy.

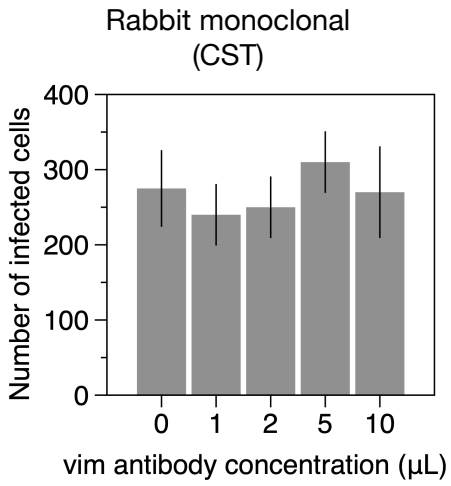

SI Fig. 3. Results from the anti-vimentin rabbit monoclonal antibody from Cell Signaling Technologies does not block uptakes of SARS-CoV-2 VLP in HEK 293T-hsACE2 cells.

"Vimentin binds to SARS2 spike protein and antibodies targeting extracellular vimentin block uptake of SARS2 virus-like particles" : Supplemental Information for Initiation of Endocytosis Modeling

To test the notion that extracellular vimentin bound to the cell membrane can initiate endocytosis of the SARS2 virus, we developed a multiscale, coarse-grained molecular dynamics-based computational model. The model consists of a cell membrane, extracellular vimentin (ECV), the angiotensin-converting enzyme 2 (ACE2), and a virus containing spike proteins.

The cell membrane is modeled as a self-avoiding, tethered sheet with fixed connectivity as shown in Fig. [1]. It is a network of equilateral triangles consisting of particles as N nodes and tethers to connect them. The two-dimensional sheet is embedded in three-dimensional Euclidean space. To suppress the crumpling transition of the membrane, we introduce self-avoidance to the system by satisfying the condition $l_o/\sigma_o < \sqrt{3}$, where l_o is the edge length of a triangle in the mesh and σ_o is the diameter of a particle [1]. Stretchability of the membrane is encoded in nearest-neighbor harmonic springs with the energy

$$E_S^{Mem} = \frac{K_{NN}^{Mem}}{2} \sum_{<ij>} \left(r_{ij} - l_o\right)^2, \tag{1}$$

with spring constant K_{NN}^{Mem} and $< ij >$ represents the sum over nearest-neighbor nodes i and j. We also have an explicit bending rigidity modeled by adding another harmonic spring between every second nearest neighbor of each node [2, 3] having energy

$$E_B^{Mem} = \frac{K_{SNN}^{Mem}}{2} \sum_{<ijk>} \left(r_{ijk} - \sqrt{3}l_o\right)^2, \tag{2}$$

with $< ijk >$ denoting second-nearest neighbors. Spring constant K_{SNN}^{Mem} can be converted to a bending rigidity .

Given the experimental findings of non-filamentous extracellular vimentin bound to the cell membrane, we focus on extracellular vimentin tetramers [4]. The extracellular vimentin tetramers are represented as semiflexible filaments, containing both springs between two consecutive monomers with spring constant, K_{NN}^{Vim}, and angular springs between three consecutive monomers to capture the bending rigidity with angular spring constant, K_{Ang}^{Vim}. The energy for each monomer triplet is, therefore,

$$E_{Ang}^{Vim} = \frac{K_{Ang}^{Vim}}{2} \left(\cos(\theta_{lmn}) - 1\right)^2, \tag{3}$$

where l, m, n denote three consecutive monomers along the filament. For simplicity, we have assumed the ACE2 receptor is the same length as the vimentin tertramers and is also a semiflexible filament with corresponding two-body springs and angular springs, K_{NN}^{ACE2} and K_{Ang}^{ACE2}, respectively. The ACE2 receptor is stiffer than vimentin and provides stability during the wrapping process. Both the vimentin tetramers and the ACE2 receptor are also connected with the membrane via springs as shown in Fig. [2] with the same two-body spring constant, which gives them the freedom to bend at any angle with respect to the membrane. We place extracellular vimentin randomly on the membrane with coverage ϕ_{Vim}, whereas ACE2 is located at the center of the membrane. The extracellular vimentin now becomes cell surface vimentin.

The virus is modeled as a deformable shell with spikes. The shell is constructed as a Fibonacci sphere, where particles/monomers are placed on the sphere in a spiral. We use a Delaunay triangulation to find triangles amongst the particles and their corresponding edges. These particles are also connected via nearest-neighbor harmonic springs each with spring constant K_{NN}^{Virus} to arrive at a tethered spherical membrane with fixed connectivity. Spike proteins are homogenously placed on the shell surface as shown in Fig. [3]. The spike protein filaments also have harmonic spring potential between two consecutive monomers with spring constant K_{NN}^{Spike}. Their bending rigidity is also coded via 3-body, or angular, spring with spring constant, K_{Ang}^{Spike}. The spike protein filaments can take any angle with respect to the virus [5, 6].

To take into account excluded volume interactions, we implement a soft-core repulsion spring between all monomers via energy

$$V_{Repel} = \begin{cases} \frac{K_{Repel}}{2} \left(r_{ij} - \sigma_o\right)^2 & r \leqslant \sigma_o \\ 0 & r > \sigma_o. \end{cases} \tag{4}$$

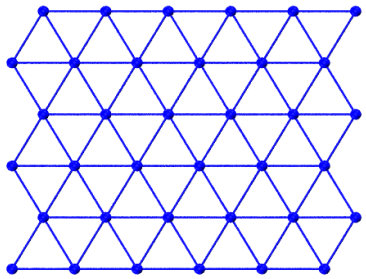

FIG. 1. *Tethered membrane as a cell membrane.* Blue particles denote the nodes of the triagular mesh and blue lines denote the tethers.

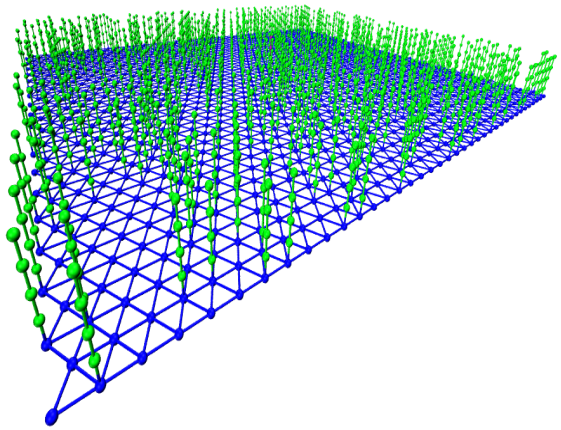

FIG. 2. *Cell membrane with bound extracellular vimentin.* Extracellular vimentin (ECV) tetramers are denoted in green. ECV tetramers are randomly attached to the cell surface to become cell surface vimentin. The coverage of extracellular vimentin depicted here is $\phi_{Vim} = 0.4$, i.e., 40 percent of the membrane nodes have bound ECV.

As for other interactions, the spike-ACE2 interaction is modeled as a stiff harmonic spring between the two filament ends with spring constant $K_{NN}^{ACE2-Spike}$ since ACE2 has a high affinity to the spike protein [7, 8]. Additionally, there is an attractive Lennard-Jones potential between the spike protein and the cell surface vimentin with a higher cut-off at $2\sigma_o$ as given by

$$V_{LJ} = \begin{cases} 4\epsilon \left[\left(\frac{\sigma_o}{r_{ij}}\right)^{12} - \left(\frac{\sigma_o}{r_{ij}}\right)^{6} \right] & r \leqslant 2\sigma_o \\ 0 & r > 2\sigma_o. \end{cases} \tag{5}$$

To convert our simulation units to biological units, we use 1 simulation unit length $= 10\,nm$, 1 unit simulation time$= 10^{-3}\,s$ and 1 unit force $= 10^{-1}\,pN$. From these scales, we can define all the parameters in biological units. The diameter of the virus is $100\,nm$, which is very similar to our own DLS measurements and similar to SARS2 [9–11]. The size of the virus is small compared to the size of the cell, typically $\sim 20\ \mu m$ in diameter, which is about 200 times bigger than the virus. Thus, during endocytosis, the virus is interacting with a small patch of the cell membrane. Hence, we simulated a tethered sheet of $length \times width = 55\,nm \times 480.6\,nm$, which is a small surface area of the cell

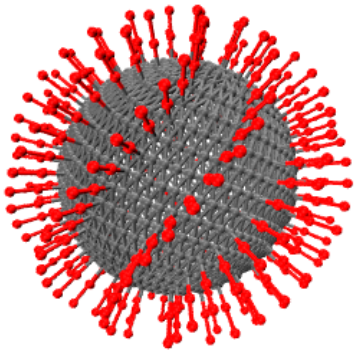

FIG. 3. *SARS2 virus.* Spike proteins are placed homogeneously on the surface of the virus.

membrane. This cell surface is covered with cell surface vimentin tetramers of length $40\,nm$, which is slightly smaller than the more typical $60-90\,nm$. We vary the density of the extracellular vimentin (ECV) to quantify its effect on viral uptake. The number of spike proteins on the viral surface can be different based on virus size [12]. We consider 200 spikes[9, 11, 13, 14] on the virus each of length $20\,nm$ [5, 9, 15] and diameter $10\,nm$ [11], to which ECV can attach. The bending rigidity of cell membrane is approximately $40k_BT$ based on the scales we have defined. Finally, each simulation was run for 10^8 simulation time units, which corresponds to $50\,s$ with recording trajectory data every $25\,ms$. See Table 1 for the parameters used in the simulations.

For each set of parameters, 10 realizations were computed and used to compute average quantities such as the fraction of spike proteins bound to ECV and the radius of gyration of the cell membrane to quantify the extent of the initiation of endocytosis, or wrapping, of the virus by ECV.

[1] Y. Kantor, M. Kardar, and D. R. Nelson, Physical Review Letters **57**, 791 (1986).
[2] D. Boal, E. Levinson, D. Liu, and M. Plischke, Physical Review A **40**, 3292 (1989).
[3] M. Plischke and D. Boal, Physical Review A **38**, 4943 (1988).
[4] B. Hwang and H. Ise, Genes to Cells **25**, 413 (2020).
[5] H. Yao, Y. Song, Y. Chen, N. Wu, J. Xu, C. Sun, J. Zhang, T. Weng, Z. Zhang, Z. Wu, L. Cheng, D. Shi, X. Lu, J. Lei, M. Crispin, Y. Shi, L. Li, and S. Li, Cell **183**, 730 (2020).
[6] B. Turoová, M. Sikora, C. Schürmann, W. J. Hagen, S. Welsch, F. E. Blanc, S. von Bülow, M. Gecht, K. Bagola, C. Hörner, G. van Zandbergen, J. Landry, N. T. D. de Azevedo, S. Mosalaganti, A. Schwarz, R. Covino, M. D. Mühlebach, G. Hummer, J. Krijnse Locker, and M. Beck, Science (New York, N.Y.) **370**, 203 (2020).
[7] D. Wrapp, N. Wang, K. S. Corbett, J. A. Goldsmith, C. L. Hsieh, O. Abiona, B. S. Graham, and J. S. McLellan, Science **367**, 1260 (2020).
[8] E. S. Brielle, D. Schneidman-Duhovny, and M. Linial, Viruses **12** (2020).
[9] S. Klein, M. Cortese, S. L. Winter, M. Wachsmuth-Melm, C. J. Neufeldt, B. Cerikan, M. L. Stanifer, S. Boulant, R. Bartenschlager, and P. Chlanda, Nature Communications **11**, 1 (2020).
[10] N. Zhu, D. Zhang, W. Wang, X. Li, B. Yang, J. Song, X. Zhao, B. Huang, W. Shi, R. Lu, P. Niu, F. Zhan, X. Ma, D. Wang, W. Xu, G. Wu, G. F. Gao, and W. Tan, New England Journal of Medicine **382**, 727 (2020).
[11] B. W. Neuman, B. D. Adair, C. Yoshioka, J. D. Quispe, G. Orca, P. Kuhn, R. A. Milligan, M. Yeager, and M. J. Buchmeier, Journal of Virology **80**, 7918 (2006).
[12] B. W. Neuman, G. Kiss, A. H. Kunding, D. Bhella, M. F. Baksh, S. Connelly, B. Droese, J. P. Klaus, S. Makino, S. G. Sawicki, S. G. Siddell, D. G. Stamou, I. A. Wilson, P. Kuhn, and M. J. Buchmeier, Journal of Structural Biology **174**, 11 (2011).
[13] M. Ponga, Scientific Reports **10**, 2 (2020).
[14] Z. Ke, J. Oton, K. Qu, M. Cortese, V. Zila, L. McKeane, T. Nakane, J. Zivanov, C. J. Neufeldt, B. Cerikan, J. M. Lu,

Parameters	Value	Reference
K_{NN}^{Mem}	$1\,pN/nm$	[16] [17]
K_{SNN}^{Mem}	$0.1\,pN/nm$	[18] [19]
K_{NN}^{Virus}	$50\,pN/nm$	SARS Cov-2[20], Brone mosaic virus [21] ,influenza virus[22] , Human Adenovirus [23] Deformable NP[24]
K_{NN}^{Spike}	$0.1\,pN/nm$	[25]
K_{NN}^{Vim}	$1\,pN/nm$	[26]
K_{NN}^{ACE2}	$5\,pN/nm$	-
$K_{NN}^{ACE2-Spike}$	$5\,pN/nm$	[27]
K_{Ang}^{ACE2}	$500k_BT$	-
K_{Ang}^{Vim}	$100k_BT$	-
K_{Ang}^{Spike}	$100k_BT$	-
ϵ	$10k_BT$	-
K_{Repel}	$1\,pN/nm$	-

TABLE I. Table of parameters used unless otherwise specified.

J. Peukes, X. Xiong, H. G. Kräusslich, S. H. Scheres, R. Bartenschlager, and J. A. Briggs, Nature **588** (2020).

[15] D. Cavanagh, Coronaviruses with Special Emphasis on First Insights Concerning SARS , 1 (2005).

[16] C. E. Morris and U. Homann, Journal of Membrane Biology **179**, 79 (2001).

[17] P. Chugh, A. G. Clark, M. B. Smith, D. A. Cassani, K. Dierkes, A. Ragab, P. P. Roux, G. Charras, G. Salbreux, and E. K. Paluch, Nature Cell Biology **19**, 689 (2017).

[18] J. Eid, H. Razmazma, A. Jraij, A. Ebrahimi, and L. Monticelli, Journal of Physical Chemistry B **124**, 6299 (2020).

[19] R. Dimova, Advances in Colloid and Interface Science **208**, 225 (2014).

[20] B. Kiss, Z. Kis, B. Pályi, and M. S. Z. Kellermayer, bioRxiv , 2020.09.17.302380 (2020).

[21] C. Zeng, M. Hernando-Pérez, B. Dragnea, X. Ma, P. Van Der Schoot, and R. Zandi, Physical Review Letters **119**, 1 (2017).

[22] I. A. Schaap, F. Eghiaia, A. Des George, and C. Veigel, Journal of Biological Chemistry **287**, 41078 (2012).

[23] P. J. de Pablo and I. A. T. Schaap, in *Advances in Experimental Medicine and Biology*, Vol. 1140 (2019) pp. 159–179.

[24] L. Chen, X. Li, Y. Zhang, T. Chen, S. Xiao, and H. Liang, Nanoscale **10**, 11969 (2018).

[25] R. A. Moreira, M. Chwastyk, J. L. Baker, H. V. Guzman, and A. B. Poma, Nanoscale **12**, 16409 (2020).

[26] Z. Qin, L. Kreplak, and M. J. Buehler, PLoS ONE **4**, e7294 (2009).

[27] C. Bai and A. Warshel, Journal of Physical Chemistry B **124**, 5907 (2020).